Petroleum Science 22 (2025) 627–640

Contents lists available at ScienceDirect

Petroleum Science

journal homepage: www.keaipublishing.com/en/journals/petroleum-science

Original Paper

Intelligent seismic AVO inversion method for brittleness index of shale oil reservoirs

Yu-Hang Sun [a, b, *], Hong-Li Dong [a], Gui Chen [c], Xue-Gui Li [a], Yang Liu [c], Xiao-Hong Yu [d], Jun Wu [d]

[a] Institute of Artificial Intelligence Energy, Northeast Petroleum University, Daqing, 163318, Heilongjiang, China
[b] College of Petroleum, China University of Petroleum (Beijing) at Karamay, Karamay, 834000, Xinjiang, China
[c] College of Geophysics, China University of Petroleum (Beijing), Beijing, 102249, China
[d] Institute of Exploration and Development, Daqing Oilfield of CNPC, Daqing, 163453, Heilongjiang, China

ARTICLE INFO

Article history:
Received 3 April 2024
Received in revised form
8 July 2024
Accepted 27 September 2024
Available online 28 September 2024

Edited by Meng-Jiao Zhou and Jie Hao

Keywords:
Brittleness index
Shale oil reservoirs
Seismic AVO inversion
TransU-net model

ABSTRACT

The brittleness index (BI) is crucial for predicting engineering sweet spots and designing fracturing operations in shale oil reservoir exploration and development. Seismic amplitude variation with offset (AVO) inversion is commonly used to obtain the BI. Traditionally, velocity, density, and other parameters are firstly inverted, and the BI is then calculated, which often leads to accumulated errors. Moreover, due to the limited of well-log data in field work areas, AVO inversion typically faces the challenge of limited information, resulting in not high accuracy of BI derived by existing AVO inversion methods. To address these issues, we first derive an AVO forward approximation equation that directly characterizes the BI in P-wave reflection coefficients. Based on this, an intelligent AVO inversion method, which combines the advantages of traditional and intelligent approaches, for directly obtaining the BI is proposed. A TransU-net model is constructed to establish the strong nonlinear mapping relationship between seismic data and the BI. By incorporating a combined objective function that is constrained by both low-frequency parameters and training samples, the challenge of limited samples is effectively addressed, and the direct inversion of the BI is stably achieved. Tests on model data and applications on field data demonstrate the feasibility, advancement, and practicality of the proposed method.

1. Introduction

With the gradual transition of the energy structure, unconventional hydrocarbon reservoirs, primarily represented by shale oil reservoirs, have emerged as key targets for oil and gas exploration and development. Despite their immense resource potential, shale oil reservoirs pose challenges due to their low porosity and permeability, making it difficult to achieve efficient shale oil extraction through natural percolation. Therefore, fracturing modification is often necessary to enhance the percolation area, ultimately improving extraction efficiency and final yield. Identifying the brittleness of shale oil reservoirs is a prerequisite for determining the fracturing locations, which are also named engineering sweet spots. The bigger the brittleness is, the more suitable the reservoirs are for fracturing modification.

The brittleness index (BI), which is used to describe the brittleness of reservoirs, is typically composed of Young's modulus, Lamé constants, shear modulus, Poisson's ratio, density, and their derived parameters. Rickman et al. (2008) studied the correlation between brittleness and Young's modulus, Poisson's ratio of reservoirs, proposing a BI represented by the normalized average of the last two parameters. Goodway et al. (2010) argued that reservoirs with higher brittleness correspond to lower Lamé constants and moderate shear modulus. They noted that an increase in Young's modulus and a decrease in Poisson's ratio are equivalent to an increase in shear modulus, and proposed using the shear modulus to directly characterize the BI. Guo et al. (2012) built upon these studies, combining Lamé constants and shear modulus to represent the BI. However, due to the unclear physical meaning of these two parameters, they replaced the parameters with Poisson's ratio, proposing a BI that only includes Poisson's ratio. Limited by the range of Poisson's ratio, the BI may not effectively identify

* Corresponding author.
E-mail address: fjsunyuhang@163.com (Y.-H. Sun).

https://doi.org/10.1016/j.petsci.2024.09.024
1995-8226/

Table 1
Parameters of the Ostrander shale model (Ostrander, 1984).

Lithology	P-wave velocity, m/s	S-wave velocity, m/s	Density, g/cm^3	Brittleness index	Young's modulus, $\times 10^7$
Sand	2438	1625	2.14	0.98	1.25
Shale	3048	1244	2.40	0.47	1.04
Sand	2438	1625	2.14	0.98	1.25

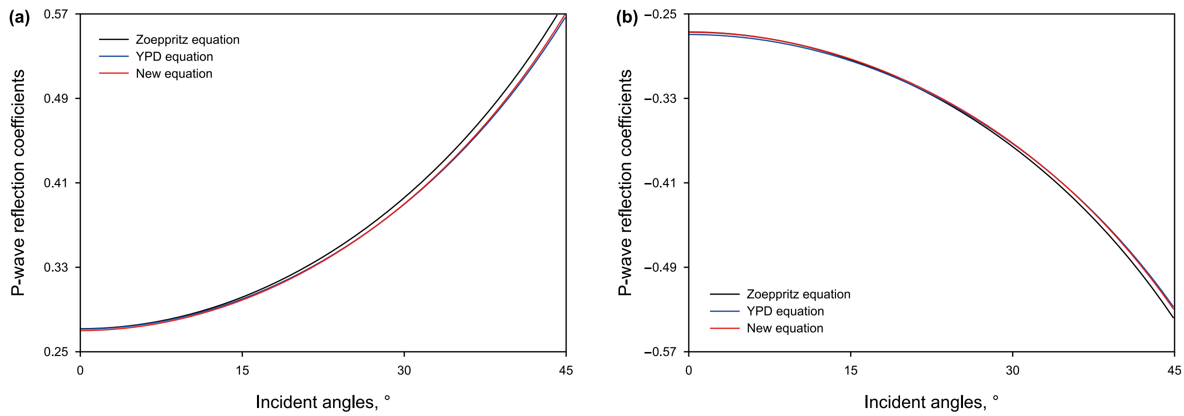

Fig. 1. P-wave reflection coefficients calculated using different AVO forward equations: **(a)** sandstone-shale interface; **(b)** shale-sandstone interface.

reservoir brittleness in some cases, resulting in certain limitations in its application. For solving the challenge, Zhang et al. (2015) proposed representing a BI as the ratio of Young's modulus to Poisson's ratio. However, without normalizing the parameters, the BI usually has a relatively large value, making it inconvenient for comparison. To address this issue, Chen et al. (2014) put forward a BI specific to shale reservoirs, represented as the ratio of Young's modulus to Lamé constants. Compared to other BIs, the BI exhibits higher accuracy in identifying shale reservoir brittleness and we primarily focus on inverting the BI here.

The brittleness index can typically be obtained through indirect and direct methods. The former first utilizes seismic and well-log data to obtain Young's modulus, Lamé constants, Poisson's ratio, and other parameters via seismic inversion methods. Subsequently, the BI is calculated using established formulas. Altamar and Marfurt (2015), and Wang et al. (2022) obtained elastic impedances through inversion, then calculated the first and second Lamé parameters, and characterized reservoir brittleness using cross plots of these parameters and density. Li et al. (2014), Liu and Sun (2015) and Han et al. (2018) both employed AVO inversion methods to obtain the former parameters for shale reservoirs, and then determined the spatial distribution characteristics of reservoir brittleness in their target work areas based on their respective evaluation criteria. Fang et al. (2023) identified the potential sensitive parameters of the chosen BI, then determined the weight coefficients of different sensitive parameters based on the analytic hierarchy process, and finally calculated the BI with high accuracy based on inverted elastic parameters. Zhang et al. (2024) proposed a multi-mineral component equivalent model suitable for complex lithologies, which can accurately calculate the ratio of P-wave velocity to S-wave velocity. Based on this, they inverted Poisson's ratio, Young's modulus and calculated a BI. Wang (2024) obtained impedance information through post-stack inversion and then realized brittleness identification based on the relationship between impedance and the chosen BI. The direct method involves first deriving an AVO forward approximation equation that directly characterizes reflection coefficients with the BI. Then, seismic AVO inversion methods are applied to directly obtain the BI. Zhang et al. (2017)

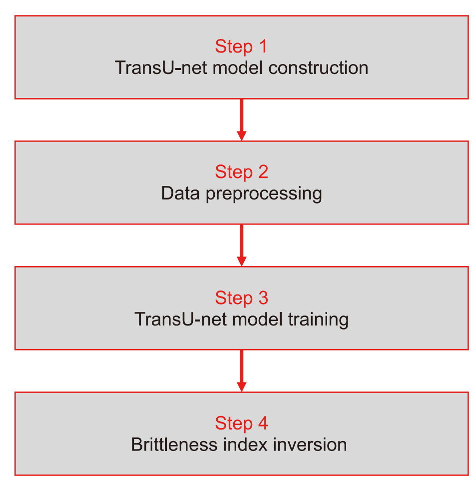

Fig. 2. The flowchart of the proposed intelligent seismic AVO inversion method.

and Li et al. (2022) independently employed the approach to directly obtain the chosen BI for their target regions. Sun et al. (2021) inverted for a BI based on an extended elastic impedance inversion method. Trial calculations in field work areas showed that the inverted BI agreed well with well-log data. Qian et al. (2020) derived a new BI equation based on the Voigt-Reuss-Hill average and obtained the BI directly through inversion. Comparatively, the direct method avoids the cumulative errors that may arise from indirect calculations, resulting in the BI with higher accuracy than the indirect one.

Based on different inversion mechanisms, seismic AVO inversion methods can be categorized into traditional and intelligent methods. Traditional methods rely on the convolution model theory, using the error between synthetic and observed seismic data as the objective function (Huang et al., 2022, 2023; Wang et al., 2022). The relationship between the objective function value and the preset iteration termination threshold controls the updating of

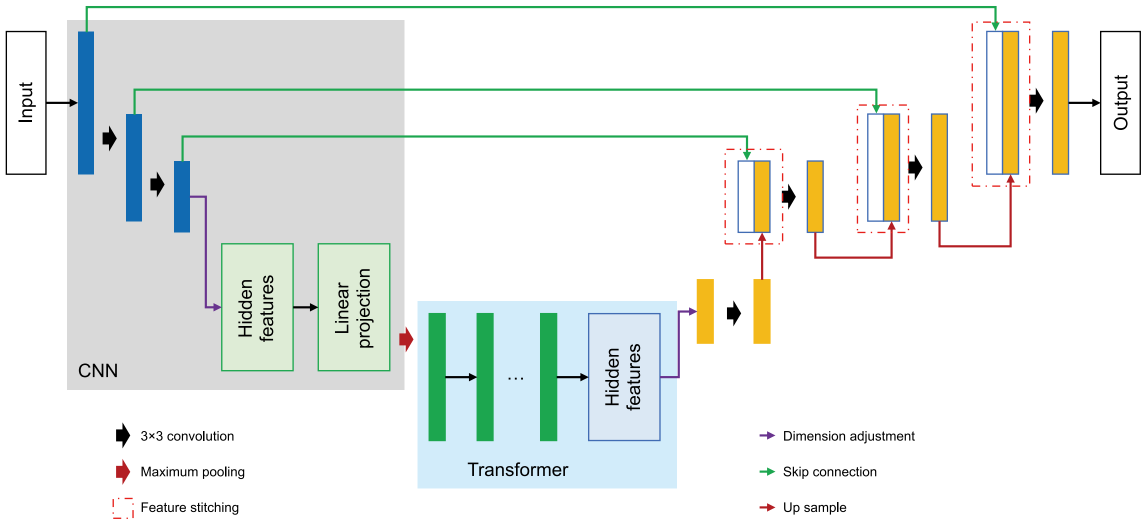

Fig. 3. The structure of the TransU-net model for brittleness index AVO inversion.

inverted parameters (Wang et al., 2021; Yu et al., 2024). Yin et al. (2015) proposed a model-constrained basis pursuit AVO inversion method that stably obtains Young's modulus and Poisson's ratio, enabling identification of reservoir brittleness. Ge et al. (2022) derived an AVO forward equation characterizing reflection coefficients in terms of Young's modulus, Poisson's ratio, and weak anisotropy parameters based on VTI media. They further improved the accuracy of inverted BI by combining the equation with Bayesian inversion theory. While these traditional methods are efficient, the accuracy of their inverted parameters often depends on the accuracy of low-frequency parameters, because observed seismic data often lack low-frequency information (Huang et al., 2024). Low-frequency parameters are usually interpolated from low-pass-filtered well-log data under the constraint of horizon information (Wang et al., 2020; Sun and Liu, 2022). However, in most field work areas, well-log data are limited and their distribution is uneven, resulting in inaccurate low-frequency parameters, which affects the accuracy of parameters inverted by traditional methods. In contrast, the accuracy of parameters inverted by intelligent methods does not rely on low-frequency parameters. These methods are based on neural network technology, where the error between the network output and sample parameters serves as the objective function (Sun et al., 2024; Sun and Liu, 2021). The relationship between the objective function value and the preset threshold controls the updating of the neural network model, which is then used to achieve parameter inversion. Chen et al. (2023) defined the BI as the ratio of Young's modulus to Poisson's ratio and derived an AVO forward approximation equation characterizing the reflection coefficient in terms of the BI. Then, they combined the equation with a gated recurrent neural network based on spatial-temporal attention mechanisms to achieve stable BI inversion. Intelligent methods are suitable for handling large-sample problems and require many representative training samples, which are typically generated from well-log data and seismic data near to wells. However, as mentioned earlier, the limited of well-log data often lead to insufficient training samples, making seismic AVO inversion being small-sample problems and affecting the accuracy of parameters inverted by intelligent methods. To address this issue, scholars studied intelligent inversion methods from the perspectives of improving neural network models and optimizing objective functions, achieving promising results. Wang et al. (2021a, 2021b) optimized neural network models, proposing intelligent AVO inversion methods based on improved residual networks and improved conditional generative adversarial networks, respectively, which improved the accuracy of inverted parameters. Sun et al. (2021) and Liu et al. (2022) combined the convolution model theory in geophysics to improve the form of the objective function, proposing intelligent methods based on multi-objective functions and spatially varying objective functions, respectively, which obtain high-accuracy parameters in small-sample cases.

To enhance the accuracy of inverted brittleness index and support engineering sweet spot identification and fracturing improvement, we propose an intelligent seismic AVO inversion method specifically tailored for brittleness index in shale oil reservoirs. Firstly, we derive an AVO forward approximation equation that directly characterizes the BI in terms of P-wave reflection coefficients. To reconcile the discrepancy between seismic AVO inversion, which is typically characterized as a small sample problem, and intelligent methods that are suited to addressing large sample problems, we construct a TransU-net model capable of extracting both local and global features. The model is designed to fit the strongly nonlinear mapping relationship between seismic data and the chosen BI. Then, we generate low-frequency parameters and training samples based on well-log data and seismic data near to wells, and then augment the latter to increase its data volume. Subsequently, we establish a combined objective function by combining the L2 norm and cross-correlation function, utilizing both training samples and low-frequency parameters to optimize the TransU-net model. The step utilizes both well-log data and seismic data information, which can alleviate the small sample problem of seismic AVO inversion to some extent. Finally, the optimized TransU-net model is employed to achieve direct BI inversion. We applied the proposed method to model data and field data from the X work area for testing and analysis, yielding several meaningful conclusions.

2. Equation derivation

2.1. Derivation of the brittleness index-based AVO forward approximation equation

The convolution model theory is the core of AVO forward modeling and inversion methods. Without considering the impact

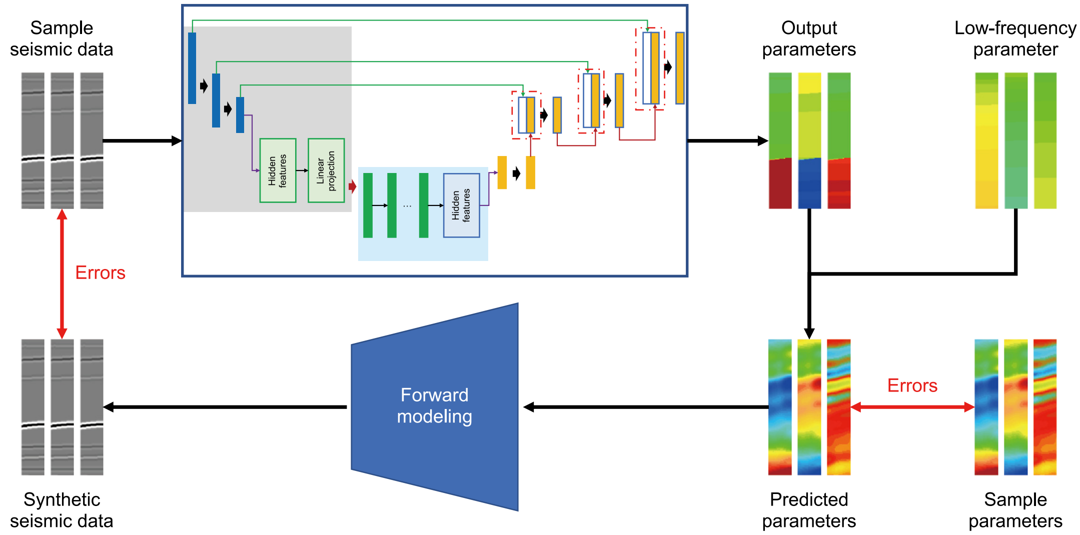

Fig. 4. The flowchart of TransU-net model training in the proposed method.

of noise, its mathematical expression is as follows:

$$\mathbf{D} = \mathbf{W}^*\mathbf{R} \tag{1}$$

where, **D** is seismic data; **W** represents the seismic wavelet; **R** denotes reflection coefficients, which are typically calculated from elastic parameters using AVO forward modeling equations. Zong et al. (2012) derived the YPD approximation equation that characterizes P-wave reflection coefficients in terms of Young's modulus and Poisson's ratio. The expression for the equation is

$$R_{\mathrm{PP}}^{1} = A\frac{\Delta E}{\overline{E}} + B_1\frac{\Delta\sigma}{\overline{\sigma}} + C\frac{\Delta\rho}{\overline{\rho}}$$

$$A = \frac{1}{4}\sec^2\theta - 2k\sin^2\theta$$

$$B = \frac{1}{4}\sec^2\theta\frac{(2k-3)(2k-1)^2}{k(4k-3)} + 2\sin^2\theta\frac{(2k-1)k}{4k-3}$$

$$C = \frac{1}{2} - \frac{1}{4}\sec^2\theta \tag{2}$$

where, R_{PP}^{1} represents the P-wave reflection coefficient; E, σ, and ρ denote Young's modulus, Poisson's ratio, and density, respectively; $\Delta\bullet$ and $\overline{\bullet}$ mean the difference and average of parameters across the interface, respectively; θ is the incident angle; k demonstrates the square of the ratio of P- and S-wave velocities. We adopt the BI proposed by Chen et al. (2014) as the inversion parameter, and its expression is as follows:

$$BI = \frac{E}{\lambda} \tag{3}$$

where, λ represents the Lamé parameter. In isotropic media, the relationship between the Lamé parameter and Young's modulus can be expressed as

$$\lambda = E\frac{\sigma}{(1+\sigma)(1-2\sigma)} \tag{4}$$

We assume that:

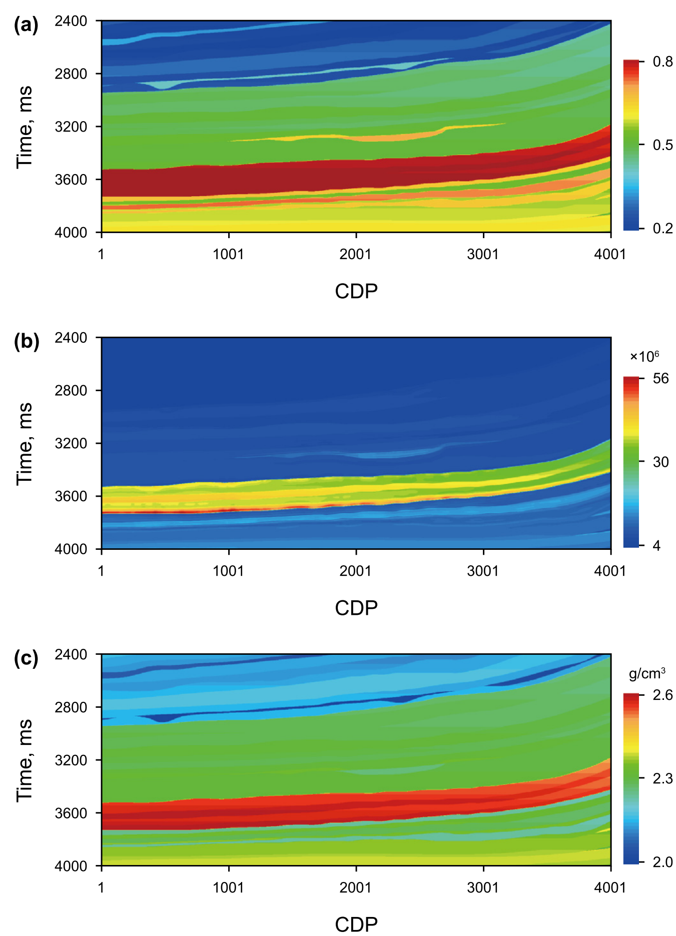

Fig. 5. Real parameters of the partial Marmousi 2 model: **(a)** brittleness index; **(b)** Young's modulus; **(c)** density.

$$\tau_1 = \frac{\sigma}{1+\sigma}$$

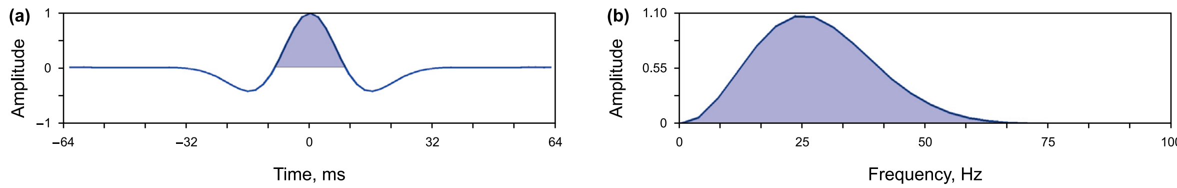

Fig. 6. Ricker wavelet with a dominant frequency of 25 Hz.

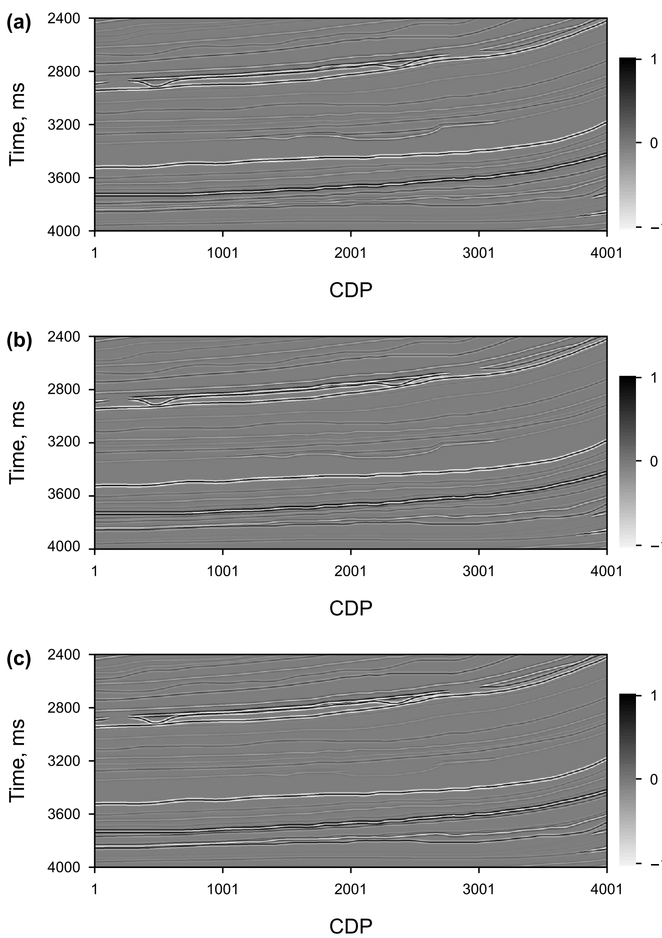

Fig. 7. Noise-free angle-stacked seismic data from the partial Marmousi 2 model: **(a)** 13°; **(b)** 23°; **(c)** 33°.

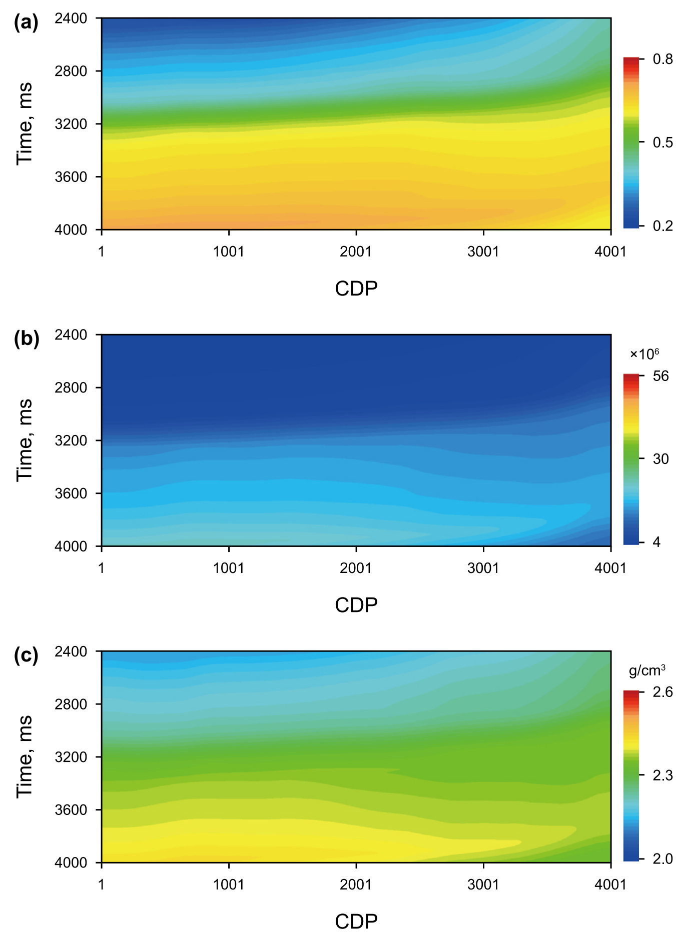

Fig. 8. Low-frequency parameters of the partial Marmousi 2 model: **(a)** brittleness index; **(b)** Young's modulus; **(c)** density.

$$\tau_2 = \frac{1}{1-2\sigma} \tag{5}$$

and there is

$$\frac{\Delta BI}{BI} = \frac{\Delta E}{E} - \frac{\Delta \lambda}{\lambda} = \frac{\Delta E}{E} - \frac{\Delta \tau_1}{\overline{\tau}_1} - \frac{\Delta \tau_2}{\overline{\tau}_2} \tag{6}$$

where,

$$\frac{\Delta \tau_1}{\overline{\tau}_1} = \frac{\Delta \frac{\sigma}{1+\sigma}}{\frac{\sigma}{1+\sigma}} = 2\frac{\frac{\sigma_2}{1+\sigma_2} - \frac{\sigma_1}{1+\sigma_1}}{\frac{\sigma_2}{1+\sigma_2} + \frac{\sigma_1}{1+\sigma_1}} = \frac{2\sigma_2 - 2\sigma_1}{\sigma_2 + \sigma_1 + 2\sigma_2\sigma_1}$$

$$\frac{\Delta \tau_2}{\overline{\tau}_2} = \frac{\Delta \frac{1}{1-2\sigma}}{\frac{1}{1-2\sigma}} = 2\frac{\frac{1}{1-2\sigma_2} - \frac{1}{1-2\sigma_1}}{\frac{1}{1-2\sigma_2} + \frac{1}{1-2\sigma_1}} = \frac{2\sigma_2 - 2\sigma_1}{1 - \sigma_2 - \sigma_1} \tag{7}$$

Due to the fact that:

$$\sigma_1 = \sigma - \frac{\Delta \sigma}{2}$$

$$\sigma_2 = \sigma + \frac{\Delta \sigma}{2}$$

$$\sigma = \frac{1-2k}{2-2k} \tag{8}$$

we have

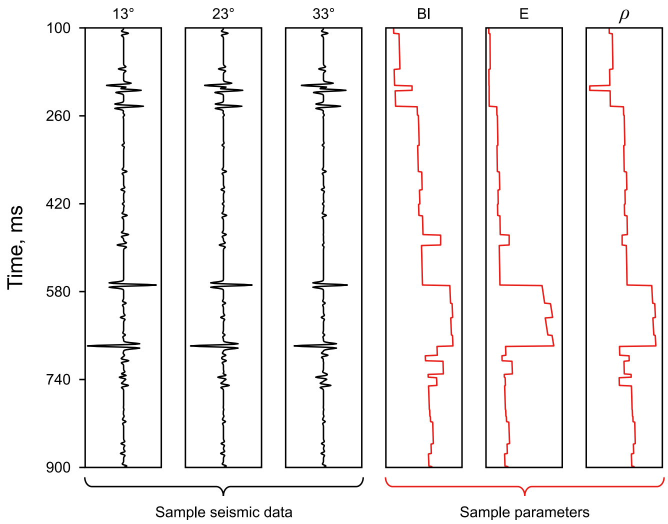

Fig. 9. Schematic diagram of a set of training samples.

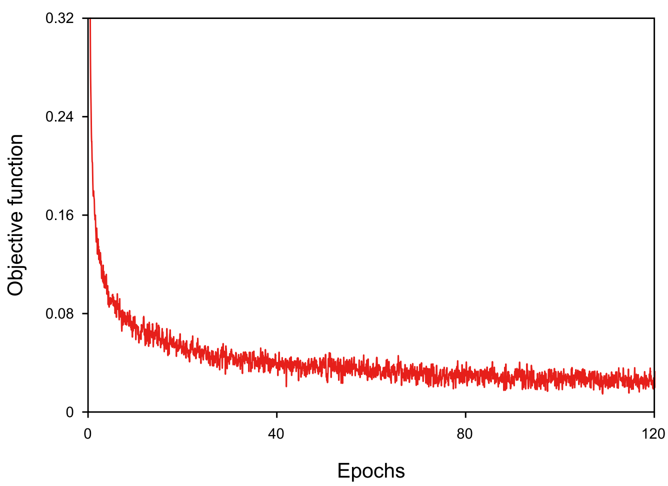

Fig. 10. The objective function curve of the network model in the proposed method.

$$\frac{\Delta\tau_1}{\tau_1} = = \frac{4\Delta\sigma}{4\sigma^2+4\sigma-\Delta\sigma^2} = \frac{1}{1+\sigma}\frac{\Delta\sigma}{\sigma} = \frac{2k-2}{4k-3}\frac{\Delta\sigma}{\sigma}$$

$$\frac{\Delta\tau_2}{\tau_2} = = \frac{2\Delta\sigma}{1-2\sigma} = \frac{2\sigma}{1-2\sigma}\frac{\Delta\sigma}{\sigma} = \frac{1-2k}{k}\frac{\Delta\sigma}{\sigma} \tag{9}$$

By substituting Eq. (9) into Eq. (6), we obtain

$$\frac{\Delta\sigma}{\sigma} = \frac{k(4k-3)}{6k^2-8k+3}\frac{\Delta BI}{BI} \tag{10}$$

And then, we substitute Eqs. (10) and (6) into Eq. (2), and obtain the AVO forward approximation equation for the P-wave reflection coefficients represented by the BI and other parameters. The expression can be shown as

$$R_{\mathrm{PP}}^2 = A\frac{\Delta E}{\overline{E}} + B_2\frac{\Delta BI}{\overline{BI}} + C\frac{\Delta\rho}{\overline{\rho}}$$

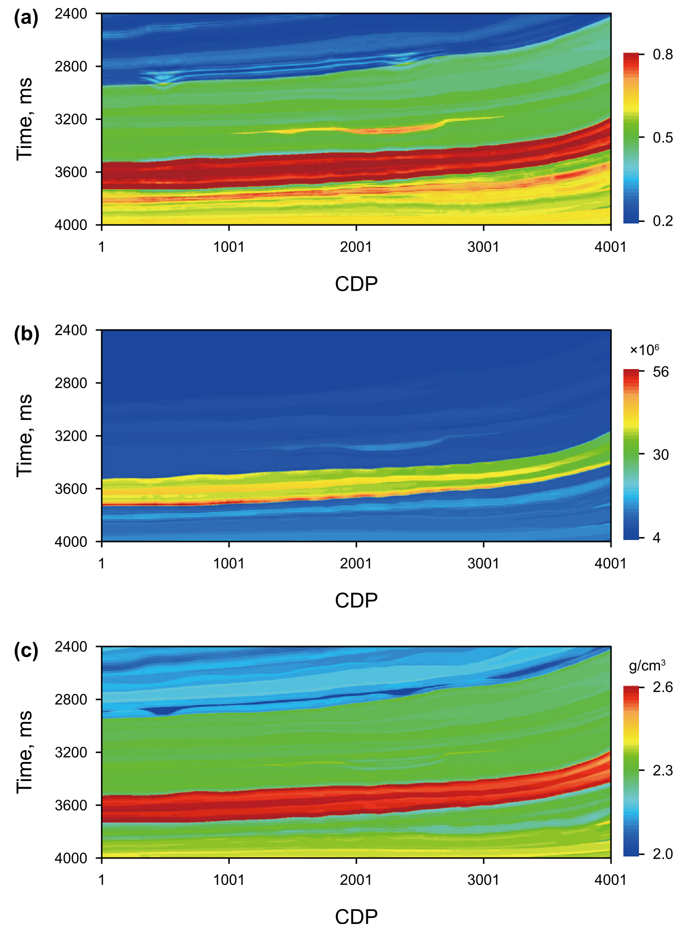

Fig. 11. Based on noise-free seismic data from the partial Marmousi 2 model, parameters inverted by the proposed method: **(a)** brittleness index, **(b)** Young's modulus, and **(c)** density.

$$B_2 = \frac{1}{4}\sec^2\theta\frac{(2k-3)(2k-1)^2}{6k^2-8k+3} + 2\sin^2\theta\frac{(2k-1)k^2}{6k^2-8k+3} \tag{11}$$

2.2. Analysis of the accuracy of the derived AVO forward approximation equation

To verify the accuracy of the derived approximation equation, we utilize the Ostrander's shale model (Ostrander, 1984), whose parameters are outlined in Table 1, to calculate the P-wave reflection coefficients using the derived approximation equation, the YPD approximation equation, and the exact Zoeppritz equation, respectively. As shown in Fig. 1, for both the sandstone-shale and shale-sandstone interfaces, when the incidence angle is less than 45°, the reflection coefficient curves calculated using the derived equation are close to those obtained from the YPD equation and the Zoeppritz equation, indicating its high accuracy and suitability for direct inversion of the brittleness index.

3. Methods

The intelligent seismic AVO inversion method for the brittleness index proposed mainly consists of four steps: TransU-net model construction, data preprocessing, TransU-net model training, and brittleness index inversion. The flowchart, which are shown in

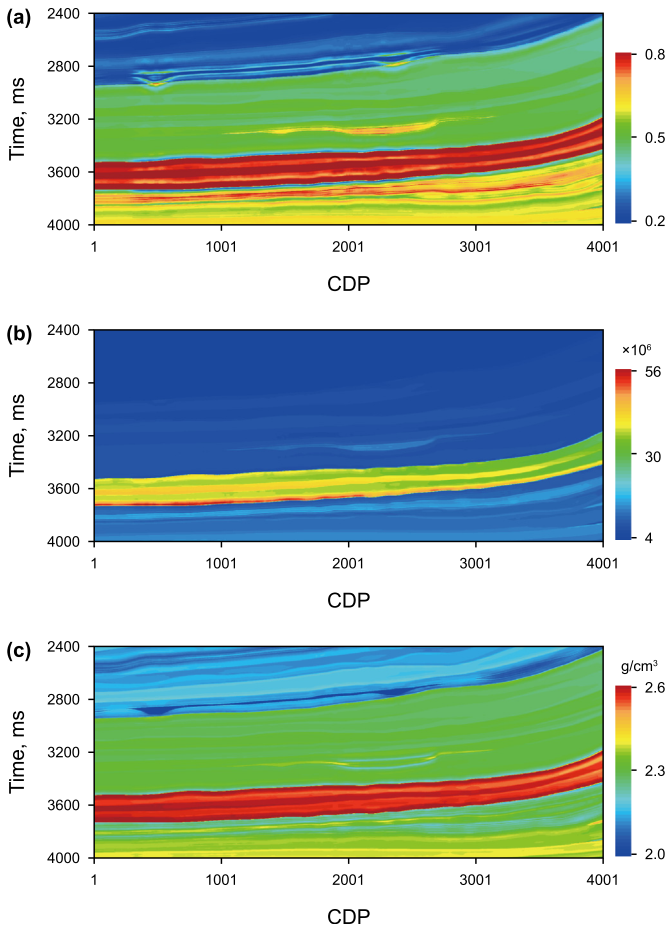

Fig. 12. Based on noise-free seismic data from the partial Marmousi 2 model, parameters inverted by the intelligent method: **(a)** brittleness index, **(b)** Young's modulus, and **(c)** density.

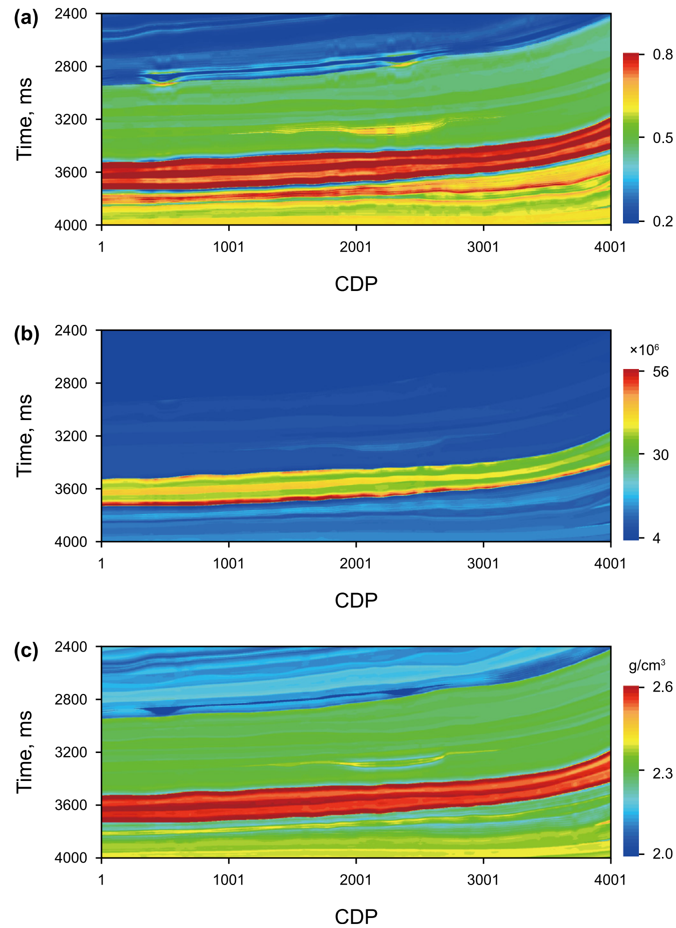

Fig. 13. Based on noise-free seismic data from the partial Marmousi 2 model, parameters inverted by the traditional method: **(a)** brittleness index, **(b)** Young's modulus, and **(c)** density.

Fig. 2, is described in detail below.

3.1. Construction of the TransU-net model

Here, we construct a TransU-net model tailored for addressing small-sample problems, as illustrated in Fig. 3. Relatively speaking, Transformer can capture global context information through its self-attention mechanism, while convolutional neural network (CNN) excels at extracting local features. TransU-net combines the advantages of both Transformer and CNN, enabling it to capture long-range dependencies in data while preserving local detailed features, thereby enhancing the comprehensiveness and accuracy of feature extraction. Furthermore, the self-attention mechanism of Transformer allows TransU-net to consider interactions between all positions in the data during feature extraction. This global perspective facilitates a better understanding of the information contained within the data. Additionally, TransU-net adopts the encoder-decoder structure of U-net and uses skip connections to fuse feature maps from the encoder and decoder, enabling feature extraction at different scales and effectively combining these features through fusion operations, thereby enhancing the richness and robustness of feature extraction. At the same time, the self-attention mechanism of Transformer also promotes interaction and fusion between features, further improving the effectiveness of feature extraction. As shown in Fig. 3, the constructed TransU-net model comprises a CNN section for extracting local information, a Transformer section for extracting global information, and an up-sampling section for restoring data features. The CNN section contains three feature maps, connected by convolution operations with a kernel size of 3×3. The last feature map is dimensionally adjusted to form local hidden features, which are then input into the Transformer section after maximum pooling. The Transformer section comprises 12 Transformer layers, consisting of multi-layer perceptions. The last Transformer layer generates global hidden features, which are dimensionally adjusted and input into the up-sampling section. The up-sampling section includes eight feature maps, connected by convolution operations and up-sample operations. After up-sampling, each feature map is concatenated with the corresponding feature map from the CNN section for feature fusion. These concatenated features are then processed by a convolution operation with a kernel size of 3×3 to generate the feature map for the next layer. In the TransU-net model, we use the ReLU activation function and set the learning rate to 0.001.

3.2. Data preprocessing

The proposed method combines the convolutional model theory with neural network technology, utilizing both low-frequency parameters and training samples. Therefore, it is necessary to preprocess seismic data and well-log data to obtain the two data. Firstly, we calculate the brittleness index and Young's modulus using well-log data, and then interpolate the calculated data and

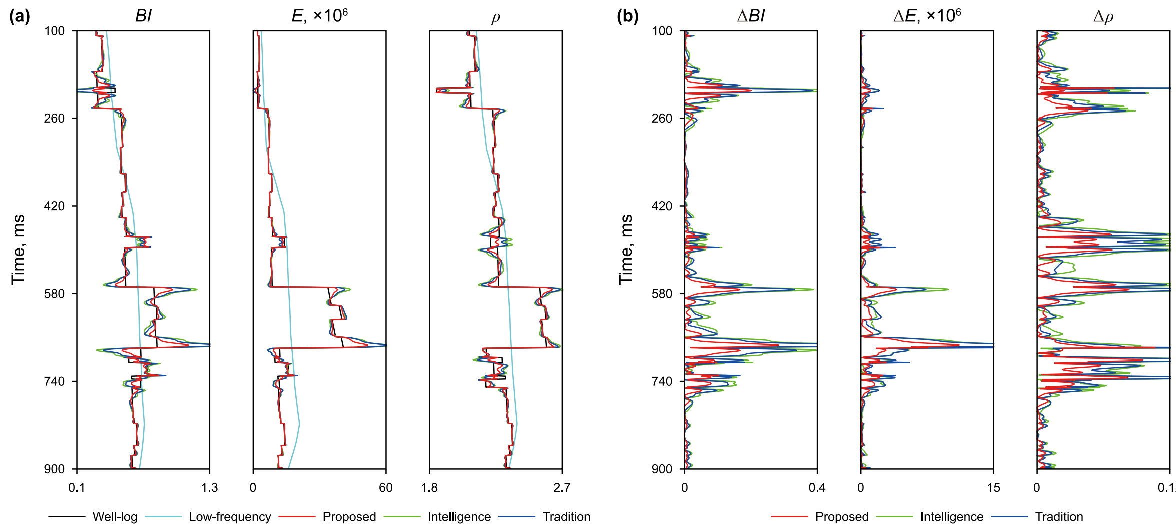

Fig. 14. Based on noise-free seismic data at CDP 2001 from the partial Marmousi 2 model, **(a)** real, low-frequency, inverted parameters, and **(b)** the absolute errors between real and inverted parameters.

Table 2
The MSEs between the real and inverted parameters and cost time of different methods.

Method	Brittleness index	Young's modulus, $\times 10^7$	Density, $\times 10^{-4}$	Cost time, s
Proposed	0.0016	1.52	4.28	581
Intelligent	0.0065	4.93	13	693
Traditional	0.0091	5.57	19	432

density after low-pass filtering to obtain low-frequency parameters under the constraint of horizon information. Subsequently, we create training samples based on the calculated data, density, and seismic data near to wells, with the former serving as the sample output (sample parameters) and the latter as the sample input (sample seismic data). Due to the limited availability of well-log data in field work areas, we enhance the number of training samples through techniques such as changing the low-frequency information of calculated data and density according geological features, distorting the high-frequency information of calculated data and density based on experience, adding random numbers on calculated data and density.

Furthermore, the AVO inversion proposed is conducted based on pre-stack angle gathers, which often involve a large volume and significantly impact computational efficiency. In field inversion tasks, we typically stack pre-stack angle gathers into different angle-stacked seismic data based on distinct angle ranges. This approach aims to enhance efficiency while preserving as much information as possible from the pre-stack seismic data across various angle ranges. When selecting the angle ranges for stacking, factors such as the maximum and minimum incident angles, as well as the signal-to-noise ratio of seismic data, are usually considered. By comprehensively evaluating the quality and angle range of both the model and the field seismic data presented in this context, we aim to achieve an optimal balance between computational efficiency and data fidelity. The pre-stack seismic data from 3° to 45° are stacked into 13°, 23°, and 33° angle-stacked seismic data according to the angle ranges of 3°–23°, 13°–33°, and 23°–43°, respectively, which are then used as the input data for inversion. Finally, statistical seismic wavelets are extracted from the seismic data for subsequent inversion.

3.3. Training of the TransU-net model

As shown in Fig. 4, the sample seismic data $\mathbf{D}_{\mathrm{Sam}}$ are first input into the constructed TransU-net model to obtain the output parameters $\mathbf{M}_{\mathrm{Out}}$. Subsequently, the low-frequency components of the output parameters are replaced with low-frequency parameters $\mathbf{M}_{\mathrm{Low}}$ to generate prediction parameters $\mathbf{M}_{\mathrm{Pre}}$. Based on the predicted parameters, P-wave reflection coefficients are calculated using Eq. (11) and then are convolved with the extracted seismic wavelets to synthesize seismic data $\mathbf{D}_{\mathrm{Syn}}$, thus creating a closed loop. Within each closed loop, we calculate the error between the predicted and the sample parameters $\mathbf{M}_{\mathrm{Sam}}$, as well as the error between the synthetic and the sample seismic data. These errors are then combined to form the objective function, which is expressed as:

$$J = \mu \cdot f_1(\mathbf{M}_{\mathrm{Pre}}, \mathbf{M}_{\mathrm{Sam}}) + (1-\mu) \cdot f_2(\mathbf{D}_{\mathrm{Syn}}, \mathbf{D}_{\mathrm{Sam}}) \tag{12}$$

where, $f_1(\cdot)$ represents the L2 norm, which is used to calculate the error between parameters; $f_2(\cdot)$ stands for the cross-correlation function, employed to measure the error between seismic data. The expression of $f_2(\cdot)$ is:

$$f_2(\mathbf{D}_{\mathrm{Syn}}, \mathbf{D}_{\mathrm{Sam}}) = \left(1 - \frac{\mathbf{D}_{\mathrm{Syn}} \cdot \mathbf{D}_{\mathrm{Sam}}}{\sqrt{\mathbf{D}_{\mathrm{Syn}}^2} \cdot \sqrt{\mathbf{D}_{\mathrm{Sam}}^2}}\right) \tag{13}$$

It enhances the noise resistance of the objective function and effectively prevents it from falling into local extrema when dealing with data exhibiting waveform characteristics; μ, which is determined through testing, denotes the weight coefficient of the first

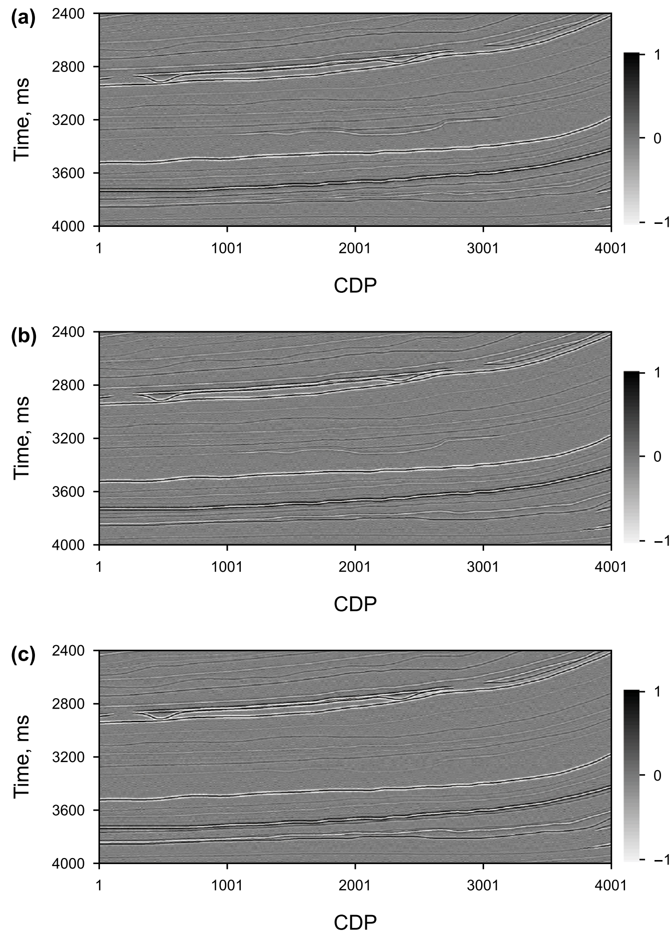

Fig. 15. Noisy angle-stacked seismic data from the partial Marmousi 2 model: **(a)** 13°; **(b)** 23°; **(c)** 33°.

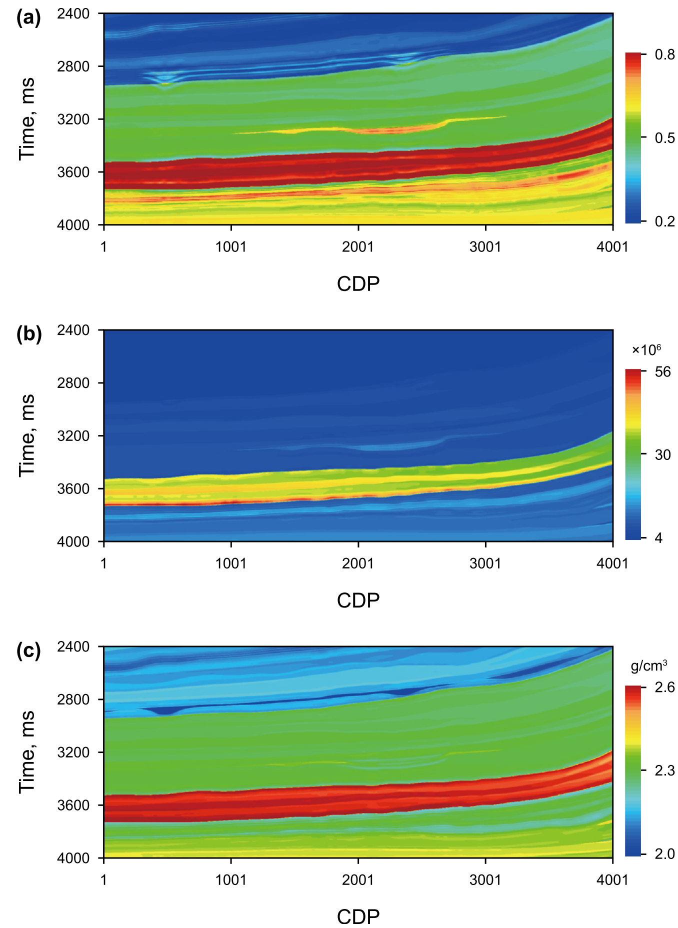

Fig. 16. Based on noisy seismic data from the partial Marmousi 2 model, parameters inverted by the proposed method: **(a)** brittleness index, **(b)** Young's modulus, and **(c)** density.

term on the right-hand side of Eq. (12), indicating the proportion of the objective function influenced by training samples.

We sequentially input the sample seismic data into the TransU-net model. In each closed loop, the objective function is calculated based on Eq. (13), and the hyperparameters of the model are iteratively updated using the backpropagation algorithm until the objective function converges, thus completing the training of the TransU-net model.

3.4. Brittleness index inversion

The angle-stacked seismic data from the target area are input into the trained TransU-net model, and low-frequency components of the output parameters are replaced with low-frequency parameters to obtain the inverted brittleness index, Young's modulus, and density.

4. Model data tests

We conduct preliminary tests using the partial Marmousi 2 model to analyze the feasibility, advancement, and noise resistance of the proposed method. The partial Marmousi 2 model comprises 4001 CDPs (common-depth points), with each CDP containing 1600 samples at a sampling interval of 1 ms. The real brittleness index, Young's modulus, and density of the partial model are presented in Fig. 5. Using these parameters, we calculate P-wave reflection coefficients based on Eq. (11) and then convolve them with the Ricker wavelet with a dominant frequency of 25 Hz (shown in Fig. 6) to synthesize pre-stack seismic data. Subsequently, the pre-stack data are stacked according to different angle ranges to obtain 13°, 23°, and 33° angle-stacked seismic data, as displayed in Fig. 7. Low-frequency parameters (shown in Fig. 8) and training samples are created using the parameters from CDPs 501, 1501, 2501, and 3501. After sample augmentation, a total of 100 sets of training samples are generated, with one set shown in Fig. 9.

4.1. Analysis of feasibility and advancement

We carry out tests using the proposed method, an intelligent method (Liu et al., 2022), and a traditional method (Shi et al., 2020). When processing the partial model data with the proposed method, we input the training samples and low-frequency parameters into the TransU-net model and follow the training process outlined in Fig. 4. Through testing, we determine the value of μ in the objective function is 0.62. After 120 iteration epochs, the objective function converges, as shown in Fig. 10. During the training process, we set aside a validation set to evaluate the performance of the TransU-net model and conducted cross-validation to prevent the model from overfitting. Here, we present the model that exhibited the best training performance. The angle-stacked seismic data shown in Fig. 5 are input into the trained TransU-net model to obtain the parameters presented in Fig. 11. As can be seen from the figures, the parameters inverted by the proposed

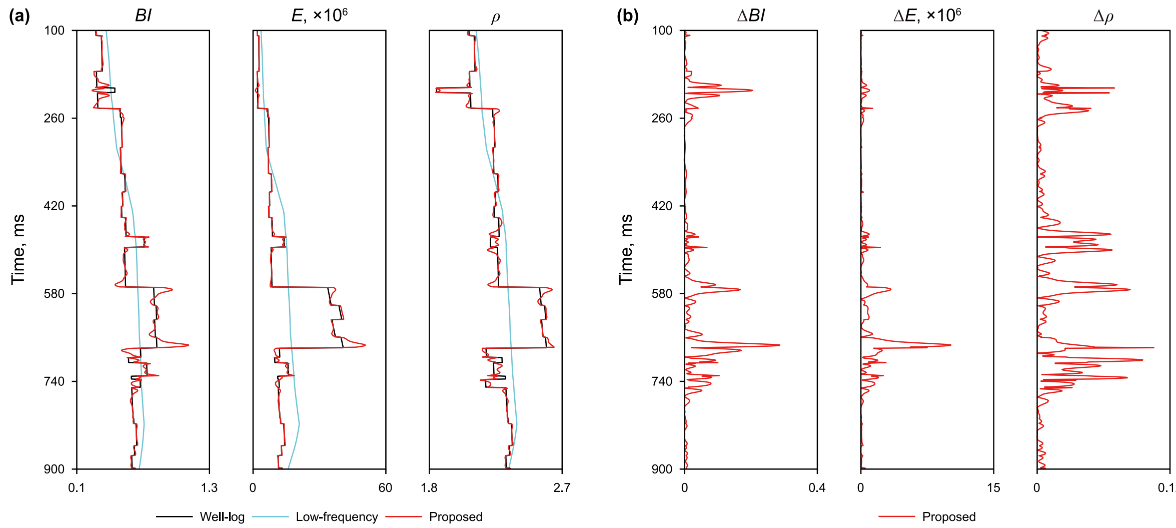

Fig. 17. Based on noisy seismic data at CDP 2001 from the partial Marmousi 2 model, **(a)** real, low-frequency, inverted parameters, and **(b)** the absolute errors between real and inverted parameters.

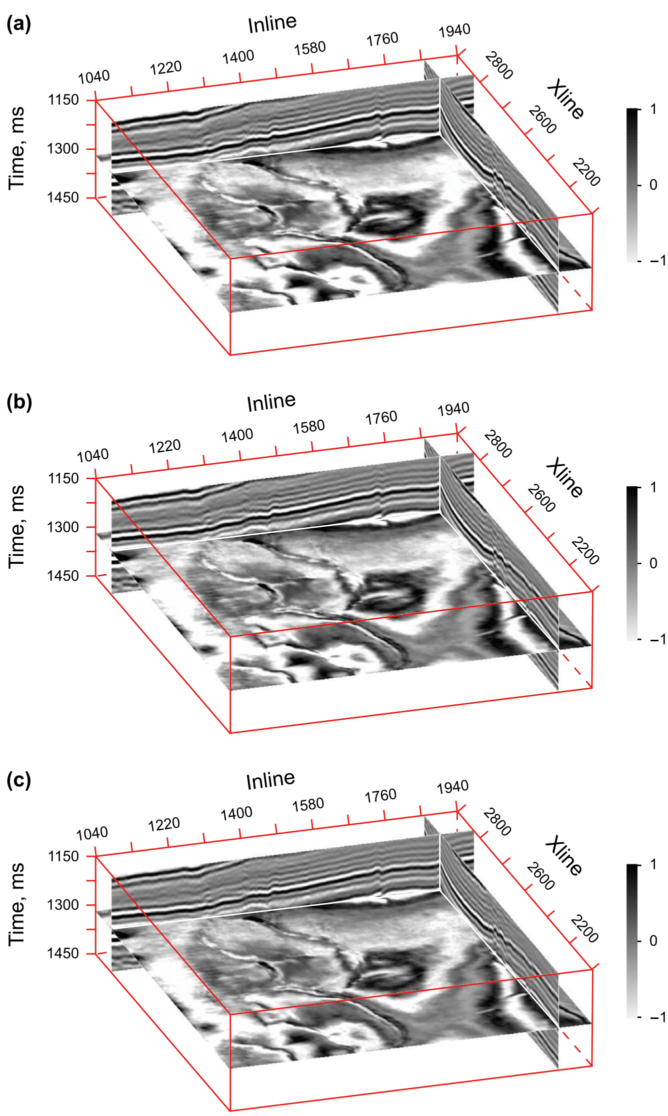

Fig. 18. Angle-stacked seismic data of the field data in the X work area: **(a)** 13°, **(b)** 23°, and **(c)** 33°.

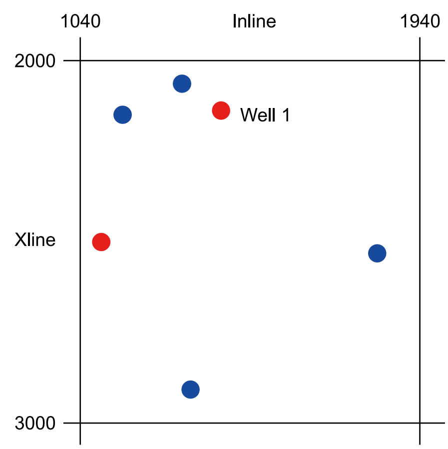

Fig. 19. Base-map of the field data in the X work area.

method tend to align with the structural patterns of the real parameters, indicating its good feasibility.

The intelligent method uses Eq. (11) as the forward modeling equation. After testing, the parameters of the network model in the method have been optimized, and the inverted parameters are shown in Fig. 12. The traditional method utilizes the low-frequency parameters displayed in Fig. 8, and its inverted parameters are presented in Fig. 13. We extract the real parameters, low-frequency parameters, and inverted parameters of the 2001th CDP and display them in Fig. 14(a). Fig. 14(b) shows the absolute values of the errors between the real and the inverted parameters. It can be observed that, compared to those of the intelligent and traditional methods, the curves of the parameters inverted by the proposed method are closer to those of the real parameters, with smaller absolute values of the corresponding errors.

To quantitatively analyze the accuracy of the parameters inverted by different methods, we calculate the mean squared errors (MSEs) between the real and the inverted parameters, and then present them in Table 2. Smaller MSEs indicate higher accuracy of the inverted parameters. As can be seen from the table, the MSEs corresponding to the parameters inverted by the proposed method are smaller than those of the intelligent and traditional

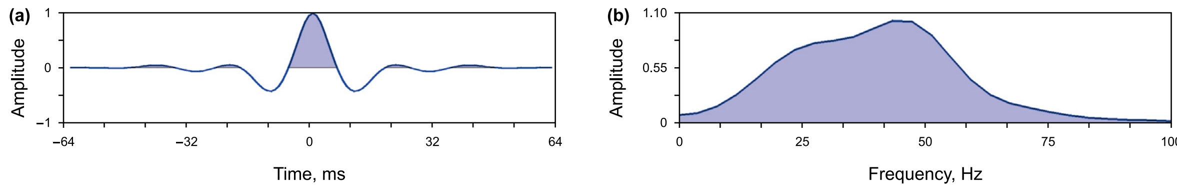

Fig. 20. Statistical seismic wavelet extracted from the field seismic data.

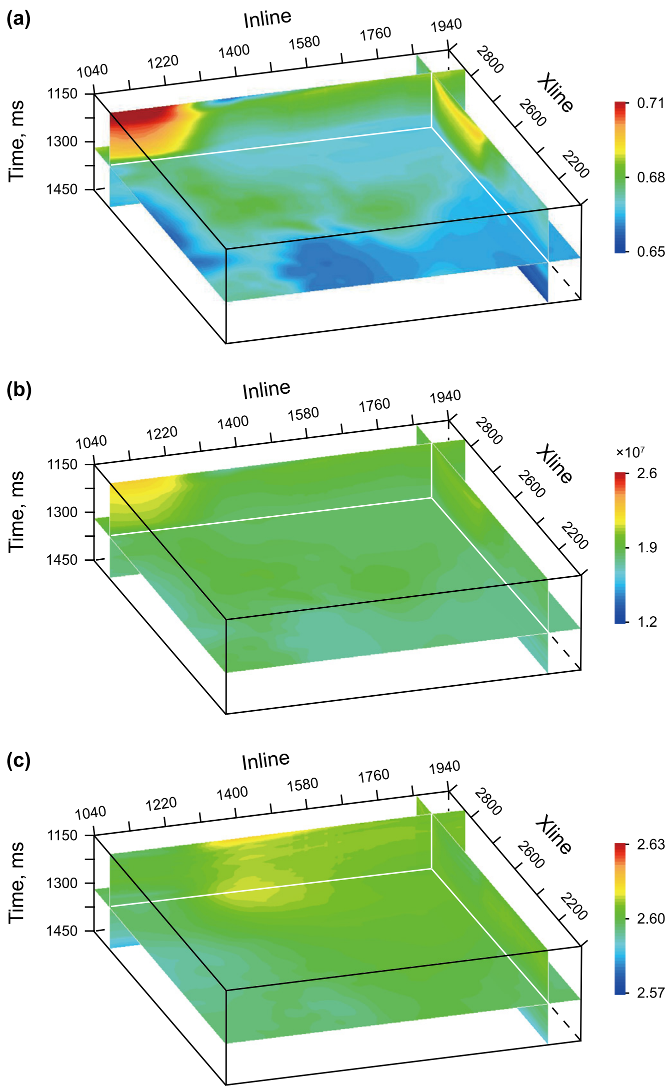

Fig. 21. Low-frequency parameters of the field data: **(a)** brittleness index, **(b)** Young's modulus, and **(c)** density.

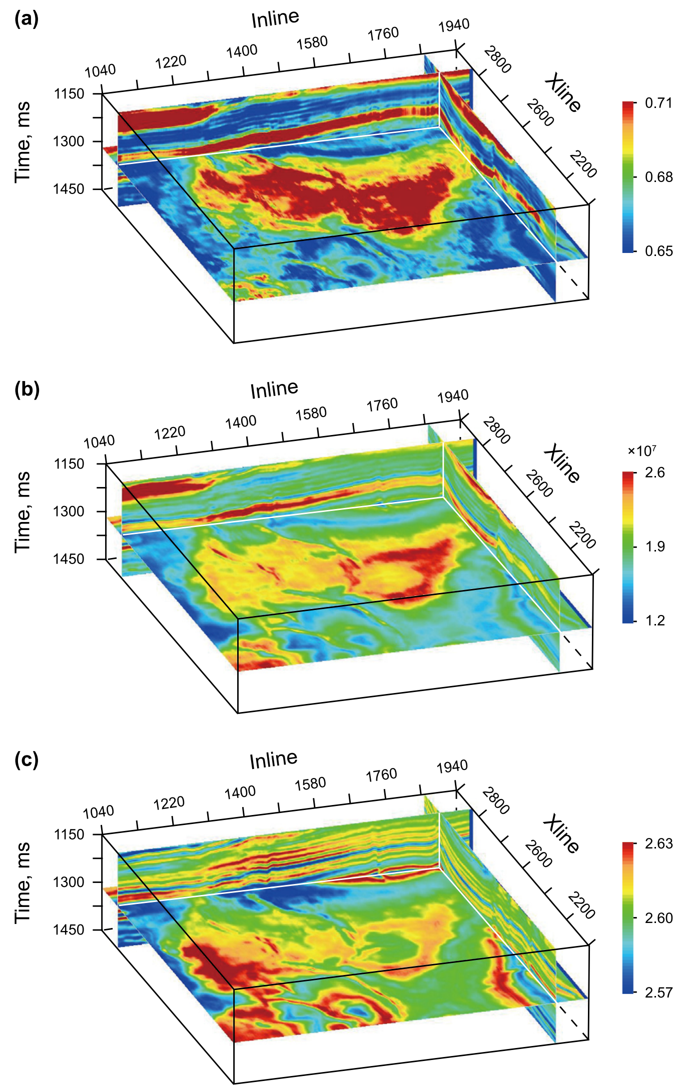

Fig. 22. Based on the field seismic data, parameters inverted by the proposed method: **(a)** brittleness index, **(b)** Young's modulus, and **(c)** density.

methods, indicating that the proposed method achieves relatively higher accuracy in inverted parameters.

Furthermore, as can be observed from Fig. 11, the inverted parameters obtained using the proposed method exhibit good lateral continuity. Generally, intelligent methods derive higher accuracy and resolution in inverted parameters for well-adjacent traces but lower accuracy and poorer lateral continuity for inter-well inverted parameters. On the other hand, traditional methods typically provide better overall lateral continuity in inverted parameters. It is because intelligent methods primarily utilize training samples created from broadband well-log data, with the objective function being the error between sample and output parameters. The kind of method is not fully leveraging seismic data with good spatial continuity characteristics. Conversely, traditional methods mainly utilize seismic data information, with the objective function being the error between synthetic and field seismic data. The proposed method combines the objective functions of both intelligent and traditional methods, using both the error between parameters and the error between seismic data. It not only utilizes the broadband information from well-log data but also leverages the spatial continuity information from seismic data. Therefore, the parameters inverted by the method exhibit both high accuracy and good lateral continuity.

Lastly, we record the time required for different methods to

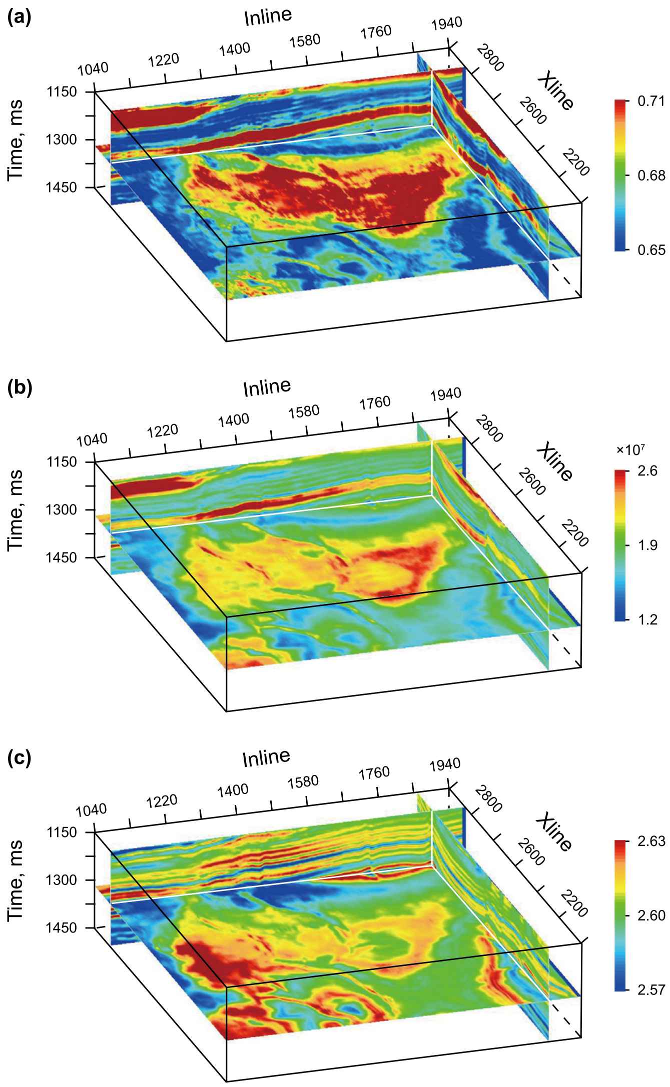

Fig. 23. Based on the field seismic data, parameters inverted by the intelligent method: **(a)** brittleness index, **(b)** Young's modulus, and **(c)** density.

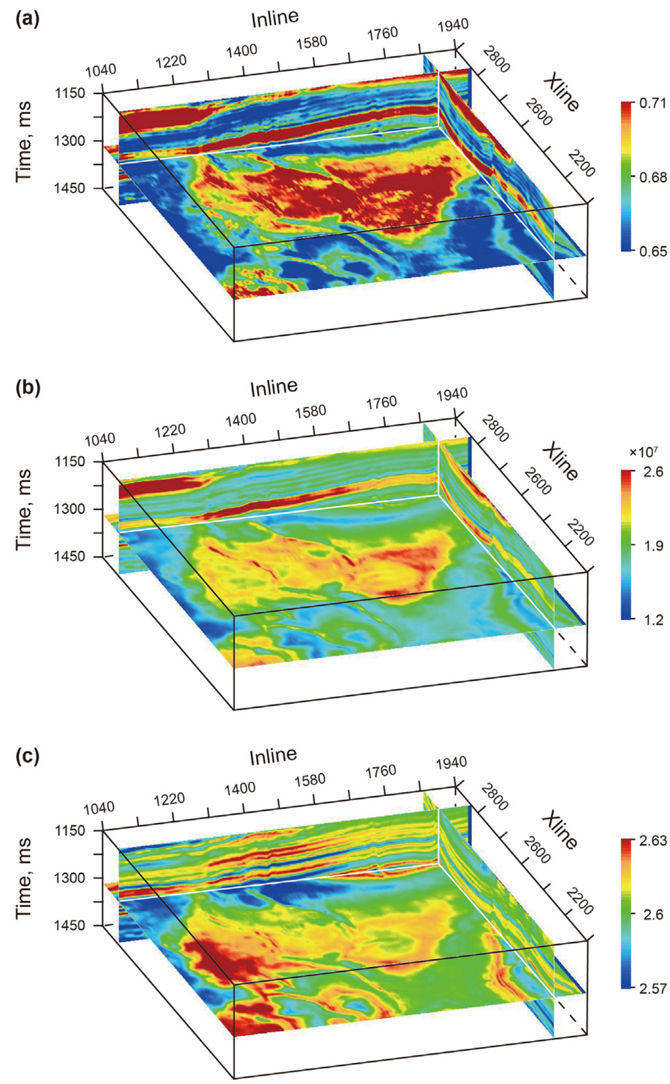

Fig. 24. Based on the field seismic data, parameters inverted by the traditional method: **(a)** brittleness index, **(b)** Young's modulus, and **(c)** density.

invert the parameters shown in Figs. 11–13, and present them in the rightmost column of Table 2. The traditional method requires the least amount of time, while the intelligent method requires the most. Although the proposed method costs more time than the traditional method, it is still within an acceptable range. Considering the accuracy, resolution, lateral continuity of inverted parameters, and efficiency comprehensively, the proposed method demonstrates advanced performance.

4.2. Analysis of noise resistance ability

We add random noise to the aforementioned synthetic prestack seismic data and then stack them to form angle-stacked seismic data with a signal-to-noise ratio of 2, as shown in Fig. 15. We directly input the noisy seismic data into the trained TransU-net model to obtain the inverted parameters as depicted in Fig. 16. It can be observed from the figures that the parameters inverted by the proposed method based on noisy seismic data still exhibit good structural consistency with the real parameters and have relatively small perturbations.

For a clear comparative analysis, we also extract the real and the inverted parameters of CDP 2001 and calculate the absolute values of their errors, as shown in Fig. 17(a) and (b), respectively. The curves corresponding to the real and the inverted parameters align well, and the absolute error curves are close to zero. Additionally, we calculate the MSEs between the two parameters, which are 0.0017 (brittleness index), 1.62×10^7 (Young's modulus), and 4.30×10^{-4} (density). Compared to inverted parameters based on noise-free seismic data, the MSEs of those based on noisy seismic data increase but remain within an acceptable range, indicating that the proposed method possesses good noise resistance capabilities.

5. Field data applications

To further validate the practicality and advancement of the proposed method, we apply it to field data from the shale oil reservoirs in the X work area. The angle-stacked seismic data of the target area, as shown in Fig. 18, comprise 900 inline and 1000 Xline, with a target layer depth ranging from 1150 to 1450 ms and a sampling interval of 1 ms. The base-map of the field data, presented in Fig. 19, indicates that the target area includes 6 wells, with blue wells designated as training wells and red wells as validation wells.

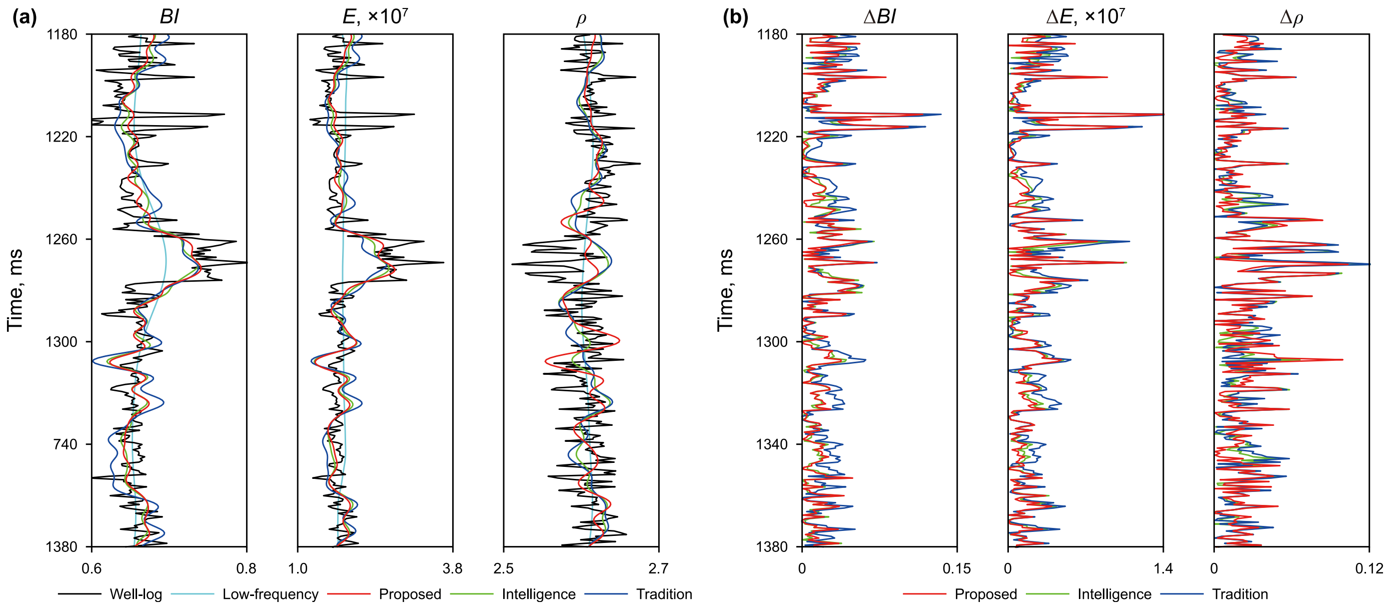

Fig. 25. Based on the field seismic data, **(a)** well-log data, low-frequency, and inverted parameters; **(b)** the absolute errors between well-log data and inverted parameters.

Table 3
The MSEs between the real and inverted parameters and cost time of different methods.

Method	Brittleness index, $\times 10^{-4}$	Young's modulus, $\times 10^{7}$	Density, $\times 10^{-4}$
Proposed	6.37	6.43	8.20
Intelligent	7.24	7.48	9.00
Traditional	9.95	10.48	9.62

Fig. 20 displays the statistical seismic wavelet extracted from the field seismic data. Based on the well-log data from the four blue wells, we first calculate the brittleness index and Young's modulus. Then, we apply a 0-0-3-5 Hz low-pass filter to the calculated data and density to obtain the low-frequency brittleness index, Young's modulus, and density. Subsequently, under the constraint of horizon information, we use the Kriging interpolation method to create the low-frequency parameters, which are depicted in Fig. 21. Following the previously mentioned data preprocessing methods, we create and augment training samples (totaling 100 sets).

The low-frequency parameters and training samples are then fed into the constructed TransU-net model. Testing reveals an μ of 0.71 in the objective function. After 170 iteration epochs, the objective function converges, completing the training of the TransU-net model. During the training process, we set aside a validation set to evaluate the performance of the TransU-net model, and to avoid it overfitting. By inputting the angle-stacked seismic data shown in Fig. 18 into the trained TransU-net model, we invert the brittleness index, Young's modulus, and density, as illustrated in Fig. 22. It can be observed that the inverted parameters exhibit structural similarity to the angle-stacked seismic data.

Additionally, we compare the proposed method with the intelligent method (Liu et al., 2022) and the traditional method (Shi et al., 2020) to analyze the advancement of our method. The intelligent method uses the same training samples as the proposed method, and its model is optimized through testing. The traditional method employs the same low-frequency parameters as our method. The parameters inverted by the two methods are shown in Figs. 23 and 24, respectively, both exhibiting good structural similarity to the angle-stacked seismic data.

To clearly assess the accuracy of the parameters inverted by different methods, we extract the well-log data, low-frequency parameters, and inverted parameters from Well 1 and present them in Fig. 25(a). Fig. 25(b) displays the absolute values of the errors between the inverted parameters and the well-log data. Compared to those of the intelligent and the traditional methods, the parameter inverted by the proposed method are generally closer to the well-log data curves, with relatively smaller absolute errors. For a quantitative comparative analysis, we calculate the MSEs between the inverted parameters and the well-log data and show the values in Table 3. The MSEs corresponding to the parameters inverted by the proposed method are lower than those of the intelligent and the traditional methods, indicating relatively higher accuracy of the parameters inverted by the proposed method.

6. Conclusions

To obtain brittleness index with high accuracy, which are vital for identifying engineering sweet spots and fracturing operations in shale oil reservoirs, we first derive an AVO forward approximation equation that directly characterizes P-wave reflection coefficients with the BI, Young's modulus, and density. Subsequently, an intelligent seismic AVO inversion method for the BI is proposed by combining the TransU-net model with the derived equation. Leveraging the ability of the TransU-net to extract both local and global information, we construct a combined objective function using the L2 norm and the cross-correlation function. By simultaneously utilizing low-frequency parameters and training samples, the proposed method effectively addresses the challenges of small-sample problem in AVO inversion. Partial Marmousi 2 model tests demonstrate the proposed method can stably invert the BI with high accuracy. Application to field data from the X work area further verifies its practicality and advancement, with inverted parameters exhibiting higher accuracy compared to other methods.

CRediT authorship contribution statement

Yu-Hang Sun: Writing – review & editing, Writing – original draft, Methodology, Data curation. **Hong-Li Dong:** Writing – review & editing, Methodology. **Gui Chen:** Methodology, Data curation. **Xue-Gui Li:** Writing – review & editing, Data curation. **Yang Liu:** Writing – review & editing, Methodology. **Xiao-Hong Yu:** Data curation. **Jun Wu:** Data curation.

Declaration of competing interest

The authors declare that they have no known competing financial interests or personal relationships that could have appeared to influence the work reported in this paper.

Acknowledgements

This study was supposed by the National Nature Science Foundation of China (Grant No. 42304131), the Natural Science Foundation of Heilongjiang Province (Grant No. LH2023D012), the Heilongjiang Postdoctoral Fund (Grant No. LBH-Z22092) and the Basic Research Fund for Universities in Xinjiang Uygur Autonomous Region (Grant No. XJEDU2023P166). The authors would like to express sincere thanks to the experts who provided help for the article.

References

Altamar, R.P., Marfurt, K.J., 2015. Identification of brittle ductile areas in unconventional reservoirs using seismic and microseismic data: application to the Barnett Shale. Interpretation 3 (4), T233–T243. https://doi.org/10.1190/INT-2013-0021.1.

Chen, J., Zhang, G., Chen, H., et al., 2014. The construction of shale rock physics effective model and prediction of rock brittleness. SEG Tech. Progr. Expand. Abstr. 2861–2865. https://doi.org/10.1190/segam2014-0716.1.

Chen, T., Gao, G., Liu, H., et al., 2023. Rock brittleness index inversion method with constraints of seismic and well logs via a CNN-GRU fusion network based on the spatiotemporal attention mechanism. Geoenergy Sci. Eng. 225, 211646. https://doi.org/10.1016/j.geoen.2023.211646.

Fang, X., Feng, H., Zhang, Z., et al., 2023. Brittleness index prediction method of tight reservoir based on grey correlation and analytic hierarchical process. Petrol. Sci. Technol. 42 (19), 2495–2519. https://doi.org/10.1080/10916466.2023.2172431.

Ge, Z., Pan, S., Liu, J., et al., 2022. Estimation of brittleness and anisotropy parameters in transversely isotropic media with vertical axis of symmetry. IEEE Trans. Geosci. Rem. Sens. 60, 5904509. https://doi.org/10.1109/TGRS.2021.3073162.

Goodway, B., Petez, M., Varsek, J., et al., 2010. Seismic petrophysics and isotropic-anisotropic AVO methods for unconventional gas exploration. Lead. Edge 29 (12), 1500–1508. https://doi.org/10.1190/1.3525367.

Guo, Z., Chapman, M., Li, X., 2012. A shale rock physics model and its application in the prediction of brittleness index, mineralogy, and porosity of the Barnett Shale. SEG Tech. Progr. Expand. Abstr. 1–5. https://doi.org/10.1190/segam2012-0777.1.

Han, X., Yang, J., Zhu, D., et al., 2018. Application of pre-stack elastic parameter inversion in the prediction of Longmaxi formation shale's brittleness. Comput. Tech. Geophys. Geochem. Explor. 40 (3), 337–344. https://doi.org/10.3969/j.issn.1001-1749.2018.03.09.

Huang, G., Ba, J., Gei, D., et al., 2022. A matrix-fracture-fluid decoupled PP reflection coefficient approximation for seismic inversion in tilted transversely isotropic media. Geophysics 87 (6), M275–M292. https://doi.org/10.1190/geo2021-0631.1.

Huang, G., Ba, J., Gei, D., et al., 2023. Amplitude variation with angle and azimuth inversion to estimate fracture properties in shale-gas reservoirs. J. Nat. Gas Sci. Eng. 111, 204919. https://doi.org/10.1016/j.jgsce.2023.204919.

Huang, G., Wei, S., Yang, C., et al., 2024. The in-situ stress prediction of a fractured shale reservoir based on AVAZ inversion: a case study from Southwest China. Geophysics 89, B415–B430. https://doi.org/10.1190/geo2023-0393.1.

Li, C., Li, Y., Guo, J., 2014. Application of geophysical technologies in the evaluation of brittleness of shale gas reservoir. Contemp. Chem. Ind. 5, 732–735. https://doi.org/10.13840/j.cnki.cn21-1457/tq.2014.05.002.

Li, L., Zhang, G., Pan, X., et al., 2022. Bayesian amplitude variation with angle and azimuth inversion for direct estimates of a new brittleness indicator and fracture density. Geophysics 87 (5), M189–M197. https://doi.org/10.1190/geo2021-0767.1.

Liu, L., Sun, Y., Liu, Y., 2022. Model-data-driven seismic inversion method based on small data. Petrol. Explor. Dev. 49 (5), 1046–1055. https://doi.org/10.1016/S1876-3804(22)60331-8.

Liu, Z., Sun, Z., 2015. New brittleness indexes and their application in shale/clay gas reservoir prediction. Petrol. Explor. Dev. 42 (1), 117–124. https://doi.org/10.1016/S1876-3804(15)60016-7.

Ostrander, W.J., 1984. Plane-wave reflection coefficients for gas sands at nonnormal angles of incidence. Geophysics 49 (10), 1637–1648. https://doi.org/10.1190/1.1441571.

Qian, K., Liu, T., Liu, J., et al., 2020. Construction of a novel brittleness index equation and analysis of anisotropic brittleness characteristics for unconventional shale formations. Petrol. Sci. 17 (1), 70–85. https://doi.org/10.1007/s12182-019-00372-6.

Rickman, R., Mullen, M., Petre, E., et al., 2008. A practical use of shale petrophysics for stimulation design optimization: all shale plays are not clones of the Barnett Shale. In: SPE Annual Technical Conference and Exhibition, SPE-115258-MS. https://doi.org/10.2118/115258-MS.

Shi, L., Sun, Y., Liu, Y., et al., 2020. High-order AVO inversion for effective pore-fluid bulk modulus based on series reversion and Bayesian theory. Energies 13 (6), 1313. https://doi.org/10.3390/en13061313.

Sun, Y., Chen, S., Li, Y., et al., 2021. Shale rocks brittleness index prediction method using extended elastic impedance inversion. J. Appl. Geophys. 188, 104314. https://doi.org/10.1016/j.jappgeo.2021.104314.

Sun, Y., Liu, Y., Dong, H., et al., 2024. Seismic AVO inversion method for viscoelastic media based on a tandem invertible neural network model. IEEE Trans. Geosci. Rem. Sens. 62, 5903418. https://doi.org/10.1109/TGRS.2024.3355481.

Sun, Y., Liu, Y., 2021. Model-data-driven AVO inversion method based on multiple objective functions. Appl. Geophys. 18 (4), 525–536. https://doi.org/10.1007/s11770-021-0915-1.

Sun, Y., Liu, Y., 2022. Model-data-driven P-wave impedance inversion using ResNets and the normalized zero-lag cross-correlation objective function. Petrol. Sci. 19 (6), 2711–2719. https://doi.org/10.1016/j.petsci.2022.09.008.

Wang, C., Yin, C., Shi, X., et al., 2022. Direct prediction method of fracturing ability in shale formations based on pre-stack seismic inversion. J. Seismic Explor. 31 (5), 407–424. http://www.geophysical-press.com/online/Vol31-5_art1.pdf.

Wang, E., 2024. Method and application of post stack seismic prediction for coal seam brittleness. Geol. Rev. 70 (1), 139–140. https://doi.org/10.16509/j.georeview.2024.s1.070.

Wang, L., Meng, D., Wu, B., 2021a. Seismic inversion via closed-loop fully convolutional residual network and transfer learning. Geophysics 86 (5), R671–R683. https://doi.org/10.1190/geo2020-0297.1.

Wang, P., Chen, X., Li, J., et al., 2020. Accurate porosity prediction for tight sandstone reservoir: a case study from North China. Geophysics 85 (2), B35–B47. https://doi.org/10.1190/geo2018-0852.1.

Wang, P., Chen, X., Li, X., et al., 2021c. Analysis and estimation of an inclusion-based effective fluid modulus for tight gas-bearing sandstone reservoirs. IEEE Trans. Geosci. Rem. Sens. 60, 4502710. https://doi.org/10.1109/TGRS.2021.3099134.

Wang, P., Cui, Y., Liu, J., 2022. Fluid discrimination based on inclusion-based method for tight sandstone reservoirs. Surv. Geophys. 43 (5), 1469–1496. https://doi.org/10.1007/s10712-022-09712-5.

Wang, Y., Wang, Q., Lu, W., et al., 2021b. Seismic impedance inversion based on cycle-consistent generative adversarial network. Petrol. Sci. 19 (1), 147–161. https://doi.org/10.1016/j.petsci.2021.09.038.

Yin, X., Liu, X., Zong, Z., 2015. Pre-stack basis pursuit seismic inversion for brittleness of shale. Petrol. Sci. 12 (4), 618–627. https://doi.org/10.1007/s12182-015-0056-3.

Yu, B., Shi, Y., Zhou, H., et al., 2024. Fast Bayesian linearized inversion with an efficient dimension reduction strategy. IEEE Trans. Geosci. Rem. Sens. 62, 3360031. https://doi.org/10.1109/TGRS.2024.3360031.

Zhang, B., Zhao, T., Jin, X., et al., 2015. Brittleness evaluation of resource plays by integrating petrophysical and seismic data analysis. Interpretation 3 (2), T81–T92. https://doi.org/10.1190/INT-2014-0144.1.

Zhang, F., Dai, Y., Zhou, D., et al., 2024. A seismic prediction method of reservoir brittleness based on mineral composition and pore structure. Front. Earth Sci. 11, 1326861. https://doi.org/10.3389/feart.2023.1326861.

Zhang, F., Jin, Z., Shen, X., et al., 2017. A direct inversion for brittleness index based on GLI with basic-pursuit decomposition. Chin. J. Geophys. 60 (10), 3954–3968. https://doi.org/10.6038/cjg20171023.

Zong, Z., Yin, X., Zhang, F., et al., 2012. Reflection coefficient equation and pre-stack seismic inversion with Young's modulus and Poisson ratio. Chin. J. Geophys. 55 (11), 3786–3794. https://doi.org/10.6038/j.issn.0001-5733.2012.11.025.